gle (≈45°) from the body at which the field perturbation is first seen is much larger than the opening angle of a Mach cone associated with the fast MHD mode for $M_s \geq M_A = 8$. This indicates the excitation of dispersive Hall-MHD modes with large group velocities (whistler-type waves). We suggest that the stripes seen in the magnetic field plot of Fig. 2 are the result of coherent interaction of such waves with wavelengths comparable to the spatial scale of the obstacle, moving away from the source region and swept back by the solar wind flow. The stripes are not seen when Hall current corrections are suppressed in the simulation. In Fig. 3, the observed and calculated variation of the magnetic field vector along the Galileo trajectory are compared. The spacecraft motion is from right to left. As seen from this plot, the model reproduces the observed field variation fairly well, in particular the two field rotations. The first rotation indicates that the spacecraft passes from the undisturbed solar wind into the region dominated both by Gaspra's deformed intrinsic field and whistler wave activity. The second rotation is associated with the current-sheet crossing. Figure 4 comprises the model predictions with respect to plasma variations along the spacecraft trajectory (proton density and proton velocity). Changing the peak magnitude of the dipole field by variation of the smoothing parameter h (within the range limited by the onset of numerical instability) does not seriously affect the results. This indicates that the particular field structure near the origin is not crucial in determining the general features of the response.

The results suggest that the solar wind interaction with Gaspra's magnetic moment produces a physical situation of intermediate character in the sense that it may be placed between the classical Mach cone type response, characteristic for point-like obstacles, and the standard magnetospheric model for large magnetized objects.

The model imposes several limitations (2D instead of 3D, non-ideal line dipole with limited peak field strength, cold ions, artificial resistivity introduced by the numerical code working on a discrete mesh) that could make our results of limited interest. The most serious of them seems to be the cut of the dipole field magnitude, required for numerical reasons. However, the fact that most of the typical features of the observations are reproduced by the simulations encourages us to believe that the model covers the basic mechanism of the interaction, and may prepare the way for 3D Hall-MHD calculations.

In summary, our results indicate that the observed magnetic field variations near Gaspra can be understood as the result of the solar wind interaction with an intrinsic magnetic moment of Gaspra of the order of 10^{14} A·m^2, tilted to the solar wind flow direction by an angle of about 45°.

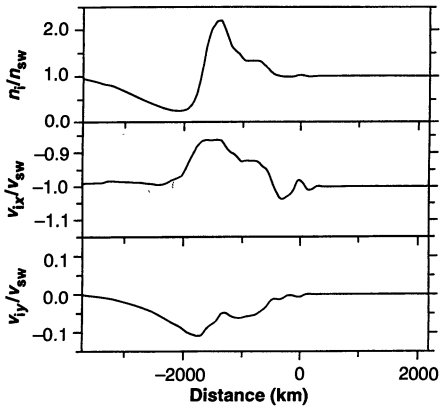

Fig. 4. Variation of proton density and velocity along the spacecraft trajectory as predicted by the simulation. Spacecraft motion from right to left, closest approach marked by zero.

REFERENCES AND NOTES

1. M. G. Kivelson *et al.*, *Science* **261**, 331 (1993).
2. J. R. Spreiter and A. Y. Alksne, *Ann. Rev. Fluid Mech.* **2**, 313 (1970).
3. R. J. Walker, T. Ogino, M. Ashour-Abdalla, in *Solar System Plasma Physics*, J. H. White Jr, J. L. Burch, R. L. Moore, Eds. (*Geophysical Monograph 54*, American Geophysical Union, Washington, DC, 1989).
4. E. W. Greenstadt, *Icarus* **14**, 374 (1971); in *Physical Studies of Minor Planets*, T. Gehrels, Ed. (NASA Sp.-267) (1971), p. 567.
5. D. L. Book, J. P. Boris, and S. T. Zalesak, in *Finite-Difference Techniques for Vectorized Fluid Dynamics Calculations*, D. L. Book, Ed. (Springer-Verlag, New York, 1981), pp. 29–41.
6. We are grateful to M. Kivelson and D. Southwood for providing a preview on the magnetometer data and for pointing us to the two papers of E. W. Greenstadt and to G. Haerendel for helpful comments.

12 August 1993; accepted 22 November 1993

Electric Field–Induced Concentration Gradients in Lipid Monolayers

Ka Yee C. Lee, Jürgen F. Klingler, Harden M. McConnell

Externally applied electric field gradients gave rise to lateral concentration gradients in monolayers of certain binary lipid mixtures. For binary mixtures of dihydrocholesterol and dimyristoylphosphatidylcholine, the application of an electric field gradient at pressures below the critical pressure produced a liquid-liquid phase separation in a monolayer that is otherwise homogenous. At pressures slightly above the critical pressure, a field gradient produced a large concentration gradient without phase separation. The lipid concentration gradients can be described by equilibrium thermodynamic chemical potentials. The observed effects appear to be relevant to the structure and composition of biological membranes.

Epifluorescence microscopy has been used to observe coexisting two-dimensional liquid phases in binary mixtures of phospholipids and steroids at the air-water interface (*1–7*). Monolayer studies of binary mixtures of phosphatidylcholines and cholesterol were initially stimulated by evidence for coexisting liquid phases in bilayers composed of these lipids and by the possibility that such coexisting phases might be significant for the structure and function of biological membranes (*8*). We devised a technique that uses an inhomogeneous electric field to manipulate lipid monolayer domains (*9, 10*). Modest electrical potentials gave rise to substantial lateral concentration gradients in lipid monolayers with compositions and properties that potentially mimic some biological membranes. The electrical field strengths were comparable with those present in biological membranes (~10^7 V/m).

We studied a binary mixture of dihydrocholesterol (DChol) and dimyristoylphosphatidylcholine (DMPC). This mixture forms two immiscible liquid phases at certain temperatures and surface pressures π and exhibits a mixing-demixing critical point (Fig. 1) (*11*). At a critical composition of $x_1 = 0.3$ (x_1 is the mole fraction of DChol), the two liquid phases, one rich in DChol and the other rich in DMPC, merge into a single phase of uniform composition at the critical point upon increase in lateral pressure or temperature (*8*). Domain sizes and shapes in the liquid-liquid coexistence region depend on competition between line tension at the domain boundary and dipole-dipole electrostatic repulsion between molecules within and between the domains (*2*).

Because of the dipole moment difference between DChol and DMPC molecules, an electric field gradient induces preferential

Department of Chemistry, Stanford University, Stanford, CA 94305–5080.

attraction and repulsion of one type of molecule over the other, and hence of one phase over the other, in the coexistence region. In this report, we describe the theoretical and experimental aspects of this electric field–induced concentration gradient in lipid monolayers.

Binary mixtures of DMPC and DChol were spread on a microfluorescence film balance (*12*). A tungsten wire (diameter, 6 μm), insulated in a glass capillary (diameter, ~20 μm), poked from the subphase for about 400 μm through the monolayer (Fig. 2). Application of an electrical potential V_0 between the subphase and the wire resulted in an inhomogeneous electric field $E(r)$ at the air-water interface. A molecule in the monolayer at a distance r from the capillary feels a force proportional to its dipole moment and the field gradient dE/dr, attractive or repulsive, depending on the polarity of V_0 and the dipole orientation (9). Because DMPC and DChol have different dipole moments, they partially separated under the influence of the electric field gradient, resulting in a concentration gradient. Three types of experiments were performed.

In type A, the monolayer (x_1 = 0.10, π = 3.0 mN/m) was in the two-phase region, well below the mixing-demixing line (point A, Fig. 1). It consisted of small domains of dark (DChol-rich) phase, interspersed fairly uniformly (because of electrostatic repulsion) through a bright (DMPC-rich) phase.

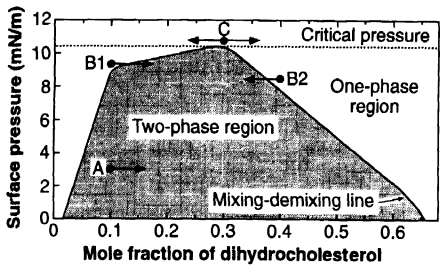

Fig. 1. Phase diagram of the DChol-DMPC system. Points A, B, and C refer to starting points of the different types of experiments that were performed. Arrows indicate local composition changes caused by electric fields. [Adapted with permission from (*11*). Copyright 1993 American Chemical Society]

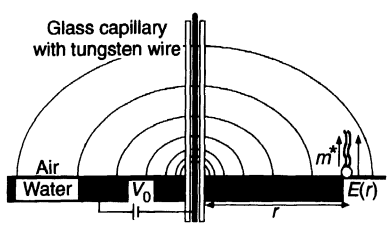

Fig. 2. Principle of the experiments. An electrical potential V_0, applied to an insulated tungsten wire, creates at the air-water interface an inhomogeneous electric field $E(r)$ that exerts a force on a lipid molecule with dipole moment m^*.

Upon application of a potential V_0 (13 to 50 V, wire negative), the dark domains were attracted to the capillary (*9*, *13*). They gathered around the capillary and fused into a single domain, which grew with time. After about 10 min, a steady state was reached because the attracted domains could no longer overcome electrostatic repulsion (Fig. 3A). Apparently, the domains grow until the field gradient on their perimeter reaches a critical value (Fig. 4A), below which the attractive force on new domains is no longer sufficient to make them fuse with the big domain.

In type B, the monolayer (x_1 = 0.10, π = 8.6 mN/m) was in the one-phase region, 0.2 mN/m above the mixing-demixing pressure but below the critical pressure (point B1, Fig. 1). Upon application of a potential V_0 (25 to 100 V, wire negative), a dark domain with a sharp edge formed around the capillary and grew with time (Fig. 3B). After about 10 min, the domain did not increase in size (Fig. 4B). If the polarity of V_0 was quickly reversed, the domain around the capillary was blown apart (Fig. 3C). The fragments, which had sharp edges, drifted away from the capillary and disappeared within 30 s. The same result was observed on the other side of the phase diagram (x_1 = 0.40, π = 8.1 mN/m) (point B2, Fig. 1) with opposite V_0 polarity: A bright domain formed around the capillary with a darker background.

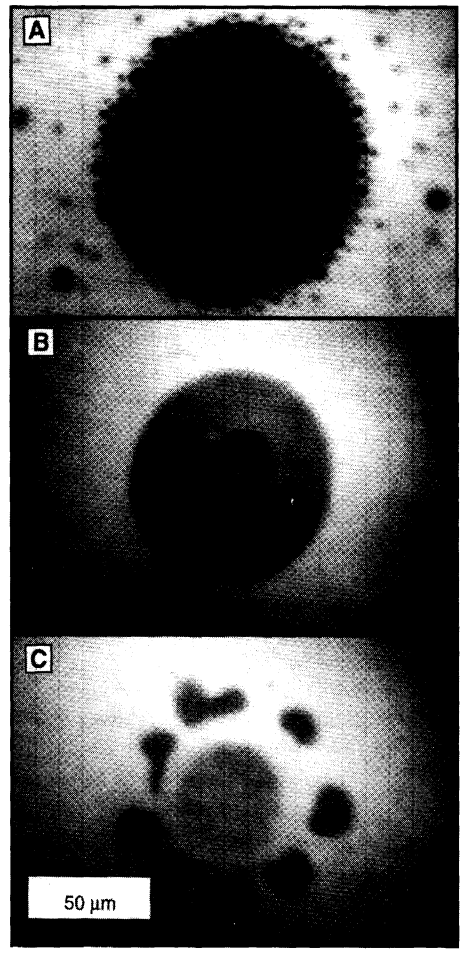

Fig. 3. Fluorescence micrographs of DChol-DMPC monolayers. (**A**) Fusion of domains in the two-phase region (type A). (**B**) Formation of a domain, starting in the homogeneous region below the critical pressure (type B1). (**C**) Same experiment (type B1) 100 ms after reversal of potential to repulsive. The previously formed domain is blown apart.

In type C, the monolayer (x_1 = 0.30, π = 10.3 mN/m) was in the homogeneous region, 0.3 mN/m above the critical pressure (point C, Fig. 1). Upon application of a potential V_0 (200 V, wire negative), a gradient in brightness developed around the capillary and reached a steady-state size within 20 s (Fig. 5A). It was continuous, with no visible boundary. Instant reversal of the polarity of V_0 resulted in expulsion of diffuse, dark regions from the capillary, which dissolved rapidly (Fig. 5B). If the reversed polarity was sustained, a diffuse bright ring formed around the capillary (Fig. 5C).

The experiments of type B and C were very sensitive to surface pressure. The magnitude of the observed effects decreased rapidly with increasing pressure so as to move away from the mixing-demixing line; special care has to be taken to maintain constant pressure during an experiment.

The effect of the inhomogeneous electric field can be understood most simply in terms of a model binary lipid mixture whose phase diagram is symmetric about a critical composition of $x_1 = x_2 = 0.5$ (Fig. 6). In this mixture, the relative proportion of the two phases remains constant as the surface pressure π is increased to the critical pressure, where the two phases merge into a homogeneous single phase. Incorporating the contribution of the electric field $E(r)$ into the chemical potential of component 1 for a

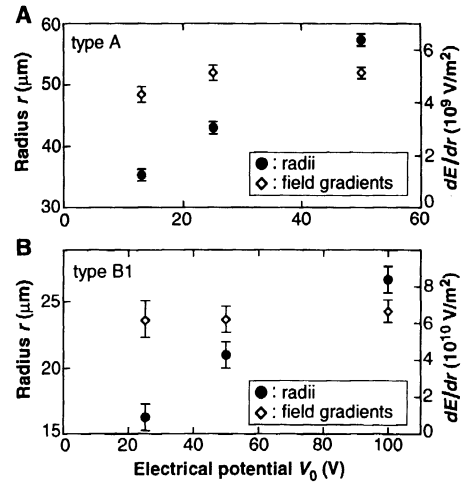

Fig. 4. Radii and calculated electric field gradients at the perimeter of steady-state domains versus applied potential for (**A**) a type A experiment and (**B**) a type B1 experiment.

model of binary mixtures (*14*), one obtains

$$\mu_1 = RT\ln x_1 + \tilde{A}_1\pi + \alpha x_2^2 - m_1\tilde{A}_1E(r) \quad (1)$$

where R is the gas constant, T and π are temperature and pressure, and m_1 and $\tilde{A}_1$ are the dipole density and molar area of component 1 (sign convention: positive E and m point into the subphase). The mixing-demixing parameter α is related to the critical temperature by $\alpha = 2RT_c$. An analogous equation can be written for the chemical potential of component 2.

If we assume ideal mixing, that $\Delta = 0$ in $\tilde{A} = x_1\tilde{A}_1 + x_2\tilde{A}_2 + \Delta x_1x_2$, and equilibrium ($\partial\mu_1/\partial r = \partial\mu_2/\partial r = 0$), the position-dependent composition varies with the field as

$$\left[\ln\left(\frac{x_2}{x_1}\right) + \frac{4T_c}{T}x_1\right]_\infty^r = -\frac{\tilde{A}_1\tilde{A}_2E(r)m}{\tilde{A}RT} \quad (2)$$

where $m = m_1 - m_2$ and $[f(r)]_\infty^r = f(r) - f(\infty)$; $x_1(r)$ refers to the mole fraction of component 1 (DChol) at distance r from the electrode and $x_1(\infty)$ the composition at large distances from the electrode.

The experimental results can be discussed in terms of the solutions to this equation (Fig. 6). For example, when $x_1(\infty) = 0.5$ and $T \approx T_c$ (upper panel) and one moves toward a positive or negative electrode, the concentration of component 1 decreases or increases as indicated by the curves. This corresponds to experiment C. Experiments of type B1 and B2 are less straightforward because of the migration of macroscopic lipid domains in electric field gradients. In Fig. 6, when $x_1(\infty)$ has the composition indicated by B1, increasing field (decreasing r) leads to a change in lipid composition until the phase boundary is reached. For still smaller values of r, only one phase is present because the other phase is repelled. The composition of the phase surrounding the electrode then varies as indicated. Note that the E versus x_1 curves in the two-phase region describe metastable and unstable states, where the maxima and minima define the spinodal.

The simple theoretical model can be used to make order-of-magnitude comparisons with experiments. For these comparisons, changing pressure changes the critical temperature according to $dT_c/d\pi = [1/(2R)]\Delta$; we estimate Δ from pressure-area-composition curves (*15*) to be on the order of -40 Å^2 per molecule, so that $dT_c/d\pi \sim -15$ K per unit pressure (millinewton per meter). In experiment C, the pressure above the critical pressure was ~0.3 mN/m, corresponding to $T - T_c \approx 4.5$°C. When $x_1 \approx 0.5$ in the model and $T - T_c \approx 4.5$°C, Eq. 2 can be used to estimate that x_1 varies as

$$x_1 = \frac{1}{2} \pm \frac{\tilde{A}_1\tilde{A}_2|E(r)m|}{4\tilde{A}R(T - T_c)} \quad (3)$$

For molecular areas on the order of 60 Å^2, m on the order of 1 D/100 Å^2 (*11*), and $E(r)$ on the order of 5×10^6 V/m ($r = 10$ μm, $V_0 = 100$ V), we obtain $x_1 = 0.5 \pm 0.05$, corresponding to significant changes in lipid composition. In a similar way, one can see from the points B1 and B2 in Fig. 1 and the model calculations in Fig. 6 that when $T < T_c$, substantial concentration gradients are brought about, and these gradients can move the lipid composition from the one-phase region into the two-phase region. When $T < T_c$ (points A, B1, and B2 in Fig. 1), the phase boundaries are sharp (Figs. 3 and 5). When the pressures are such that $T > T_c$, the boundary between the dark region (high DChol) and the light region (high phospholipid) is not sharp (Fig. 5); as expected from Fig. 6, there is no phase boundary. The sudden field-reversal, "blow-out" experiments (Figs. 3C and 5B) were carried out to demonstrate this effect. The concentration-gradient regions are expelled from the electrode and are clearly visible.

The calculations leading to Eq. 2 were simplified by setting $\Delta = 0$. When Δ is not neglected, there is an additional effect of the applied electric field in producing a gradient in the critical temperature. However, from field-reversal experiments, we conclude that the dominant effect of the electric field is the one described in Eq. 2. That is, combining a change from composition B1 to B2 (Fig. 1) with reversal of the electric field direction results in reversal of the concentration gradient, an effect not expected if the major effect of the electric field is to change T_c.

These experiments are potentially relevant to the composition, structure, and function of biological membranes. In these membranes, lipid composition and physical

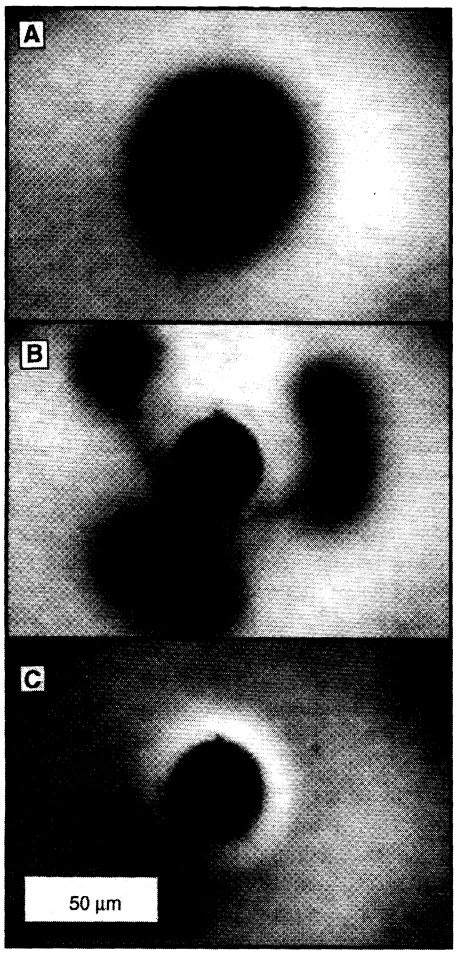

Fig. 5. Fluorescence micrographs of type C experiments. (**A**) Steady-state gradient formed above the critical pressure. (**B**) 100 ms after reversal of potential to repulsive. (**C**) Steady-state gradient formed with opposite polarity.

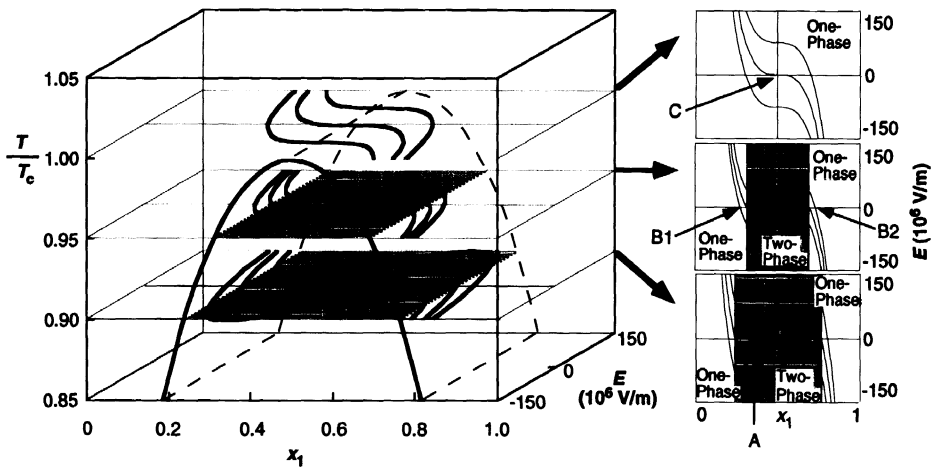

Fig. 6. Model phase diagram, extended to the third dimension in the presence of an electric field. Three cross sections ($T/T_c = 0.9$, 0.95, and 1) show how the local composition x_1 varies as a function of the electric field: Starting with a certain composition x_1 at $E = 0$, the composition change in the presence of an electric field can be found by following a curve given by Eq. 2. Three curves are shown for each temperature. Arrows A, B, and C correspond to the starting points of the experiments performed. Parameters for model calculations: $T_c = 340$ K, $m = -0.65$ D/nm^2 (*11*), and $\tilde{A} = \tilde{A}_1 = \tilde{A}_2 = 1$ nm^2 per molecule.

properties are carefully controlled (*16*), and the function of membrane proteins is modulated by these parameters (*17*). Often the growth temperatures are just above the temperatures for the onset of phase separations (*18*) and therefore may be close to lipid critical temperatures. The experiments show how proximity to a critical point allows the local lipid composition to adjust to the presence of an electric field (*19*). Electric fields are of course only one source of local intermolecular forces that play roles in lipid-protein interactions. Lipid mixtures near critical points should be responsive to many of these forces.

REFERENCES AND NOTES

1. H. Möhwald, *Annu. Rev. Phys. Chem.* **41**, 441 (1990).
2. H. M. McConnell, *ibid.* **42**, 171 (1991).
3. C. M. Knobler and R. C. Desai, *ibid.* **43**, 207 (1992).
4. S. Subramaniam and H. M. McConnell, *J. Phys. Chem.* **91**, 1715 (1987).
5. M. Seul and J. Sammon, *Phys. Rev. Lett.* **64**, 190 (1990).
6. P. A. Rice and H. M. McConnell, *Proc. Natl. Acad. Sci. U.S.A.* **86**, 6445 (1989).
7. C. L. Hirshfeld and M. Seul, *J. Phys. Paris* **51**, 1537 (1990).
8. D. J. Rectenwald and H. M. McConnell, *Biochemistry* **20**, 4505 (1981).
9. J. F. Klingler and H. M. McConnell, *J. Phys. Chem.* **97**, 2962 (1993).
10. K. Y. C. Lee and H. M. McConnell, *ibid.*, p. 9532.
11. D. J. Benvegnu and H. M. McConnell, *ibid.*, p. 6686.
12. Monolayers were spread at 21°C on a subphase of 2 mmol of KCl. Each monolayer contained 1 mole percent of the fluorescent dye Texas Red–dipalmitoyl phosphatidylethanolamine (DPPE), which preferentially associates with DMPC, making composition gradients visible. See (*9*) and (*11*) for details.
13. W. M. Heckl, A. Miller, H. Möhwald, *Thin Solid Films* **159**, 125 (1988).
14. J. G. Kirkwood and I. Oppenheim, *Chemical Thermodynamics* (McGraw-Hill, New York, 1961).
15. M. C. Phillips, *Prog. Surf. Membr. Sci.* **8**, 184 (1972).
16. M. K. Behan-Martin, G. R. Jones, K. Bowler, A. R. Cossins, *Biochim. Biophys. Acta* **1151**, 216 (1993).
17. B. Deuticke and C. W. M. Haest, *Annu. Rev. Physiol.* **49**, 221 (1987); M. Shinitzky, Ed., *Physiology of Membrane Fluidity* (CRC Press, Boca Raton, FL, 1984), vol. 1, chap. 1.
18. C. D. Linden and C. F. Fox, *Acct. Chem. Res.* **8**, 321 (1975).
19. Both the sign and the magnitude of dipole densities in lipid monolayers are consistent with the dipole moments of terminal methyl groups of lipids (*9, 11*). See also V. Vogel and D. Möbius, *Thin Solid Films* **159**, 73 (1988). These dipoles are only weakly screened in monolayers and in bilayer regions of biological membranes. The effects of electric fields on lipid distributions are then expected to be similar at comparable field gradients.

20. We are indebted to J. Brauman and J. Seelig for helpful discussions. This work was supported by the National Science Foundation (NSF DMB 90-05556) and the Deutsche Forschungsgemeinschaft (K1 834/1-1).

21 October 1993; accepted 7 December 1993

Stilbazolium-MPS_3 Nanocomposites with Large Second-Order Optical Nonlinearity and Permanent Magnetization

Pascal G. Lacroix, René Clément,* Keitaro Nakatani, Joseph Zyss, Isabelle Ledoux

Intercalated layered materials comprising an organic dye and inorganic MPS_3 [where M is either the manganese ion (Mn^{2+}) or the cadmium ion (Cd^{2+})] phases have been prepared. The intercalation process induces a spontaneous poling, giving rise to an efficiency of 750 times that of urea in second-harmonic generation for the cadmium derivative. In addition, the manganese derivative displays a permanent magnetization below 40 kelvin. Thus, these materials exhibit both a large optical nonlinearity and magnetic ordering.

Since the observation that a single crystal of quartz could frequency-double the output of a ruby laser (*1*), the search for nonlinear optical (NLO) materials has been motivated by the potential applications in many areas of optoelectronics. Although most of the currently available materials are inorganic, molecular or organic materials that exhibit a second-order NLO response that, in some cases, is several orders of magnitude higher than that of inorganic compounds have the potential to supplant inorganic crystals (*2*). However, one of the main bottlenecks to the development of new optical materials is the compulsory noncentrosymmetric environment of the chromophores if the molecular hyperpolarizability (β) is to contribute to an observable bulk nonlinear susceptibility (χ^2) (*3*). Various strategies have been reported for the engineering of molecules into acentric arrangements in single crystals (*4*) or for the poled polymer approach (*5*), in which the polarizable chromophores are oriented by a strong electric field at temperatures above the glass transition of the films.

The fact that such promising materials are not yet readily available is closely related to problems in their alignment stability over time. Hence, there is a need for alternative routes to stabilize permanently the polar order of the chromophores. Several attempts have already been performed to incorporate chromophores into organic (*6–8*) and inorganic (*9–12*) hosts to generate spontaneous poling. Efficiencies of several times that of urea were achieved even when neither the pure host nor the pure guest could frequency-double. This method could be particularly important in the case of ionic or non-dipolar guests [for example, octupolar chromophores (*13*)], as poling fields require neutral species as well as a nonzero dipole moment.

One of the largest classes of organics with large second-order polarizabilities consists in donor-acceptor–substituted stilbenes. Among them, the 4-[2-(4-dimethylaminophenyl)ethenyl]-1-methylpyridinium cation ($DAMS^+$) has been reported to exhibit one of the largest known frequency-doubling capacities (*14*).

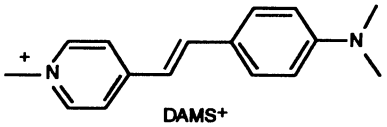

DAMS+

We found that $DAMS^+$ could be successfully intercalated by an ion-exchange process (*15–17*) into several MPS_3 (or $M_2P_2S_6$, where M = Mn^{2+} or Cd^{2+}) phases (*18*). These are a class of lamellar materials made up of M^{2+} cations and $P_2S_6^{4-}$ anions first described by Klingen and colleagues (*19*) and exhibit a great variety of properties, including magnetism (*17, 20, 21*) and metallic behavior (*22*). The intercalates were initially found to give a small second-harmonic generating (SHG) response on the order of that of urea, but these results were not conclusive: DAMS chromophores can be 10^3 times more efficient than urea (*14*), and so the poor SHG signals recorded might have originated from grain surface effects only. Also, these intercalates were not well crystallized, which could also explain low SHG efficiency.

Following our first results (*18*), we targeted an optimized intercalation process in one step by direct reaction at 130°C of MPS_3 powder with an ethanolic solution of DAMS iodide in the presence of pyridinium chloride (*23*). The role of pyridinium chloride is to generate in situ an intermediate pyridinium intercalate that undergoes rapid exchange with the DAMS species. Eventually, we synthesized two compounds of formula $Cd_{0.86}PS_3(DAMS)_{0.28}$ and $Mn_{0.86}PS_3(DAMS)_{0.28}$,

P. G. Lacroix and R. Clément, Laboratoire de Chimie Inorganique, U.R.A. 420, Bat 420, Université Paris Sud, 91405 Orsay Cedex, France.
K. Nakatani, Laboratoire de Physicochimie des Rayonnements (Equipe E.N.S. Cachan), Université Paris Sud, 91405 Orsay Cedex, France.
J. Zyss and I. Ledoux, Laboratoire de Bagneux, C.N.E.T., 92220 Bagneux, France.

*To whom correspondence should be addressed.